Available online at www.sciencedirect.com

ScienceDirect

www.elsevier.com/locate/jmbbm

Short Communication

The coefficient of friction of UHMWPE along an entire walking cycle using a ball-on-disc tribometer under arthrokinematics and loading conditions prescribed by ISO 14243-3:2014

J.D.O. Barceinas-Sanchez, M. Alvarez-Vera, L.A. Montoya-Santiyanes, I. Dominguez-Lopez, A.L. Garcia-Garcia*

Instituto Politécnico Nacional - Centro de Investigación en Ciencia Aplicada y Tecnología Avanzada Unidad Querétaro, Cerro Blanco No 141, 76090 Querétaro, Qro., Mexico

ARTICLE INFO

Article history:
Received 6 June 2016
Received in revised form
20 August 2016
Accepted 23 August 2016
Available online 30 August 2016

Keywords:
UHMWPE
ISO standard
Coefficient of friction
Sliding/rolling
Walking cycle
Ball-on-disc

ABSTRACT

The observation of tribological phenomena occurring in total knee replacement (TKR) simulators may be obscured by the intrinsic complexity of their operation: the dynamics and kinematics prescribed by the ISO 14243-3:2014 standard, and the geometry of the surfaces involved. On the other hand, evaluating the individual performance of the tribosystem elements may be carried out in simpler apparatuses. An experimental method is presented here, by means of which the arthrokinematics and loading conditions prescribed by the said standard are adapted to a ball-on-disc configuration in order to observe the behavior of the coefficient of friction along an entire walking cycle, using the contact point of an AISI 316L stainless steel ball rolling/sliding on an ultra-high molecular weight polyethylene (UHMWPE) disc, lubricated by a solution of fetal bovine serum, at 37 °C. The method was tried on two different testing fluids prepared with protein concentrations of 20 g/L, according to the said standard, and 36 g/L, as received. The statistical model obtained for the behavior of the COF during the entire walking cycle may be used in numerical simulations of UHMWPE wear, under the conditions established by ISO 14243-3:2014.

© 2016 Elsevier Ltd. All rights reserved.

1. Introduction

Total knee replacements (TKR) are highly successful implants, being wear and fatigue damage of the ultra-high molecular weight polyethylene (UHMWPE) tibial insert the limiting factor in the service life of total and unicondylar knee replacement systems (Kurtz, 2009).

As opposed to wear, a tribological effect usually characterized ex situ after several million cycles, the coefficient of friction (COF) is the immediate and natural response of all

*Corresponding author.
E-mail address: obarceinas@ipn.mx (J.D.O. Barceinas-Sanchez).

http://dx.doi.org/10.1016/j.jmbbm.2016.08.032
1751-6161/© 2016 Elsevier Ltd. All rights reserved.

tribosystems and may be correlated with instantaneous shifts in loading, surface contact, and environment conditions like lubricant temperature and pH, among others. Therefore, it should be clear, from the beginning, that the measurement performed with the method herein is not intended to measure wear; basically, because the number of cycles required to measure the COF is negligible, compared to the number required for wear measurements.

Since the indications for lower extremity joint arthroplasty have expanded to include both younger and more active patients (Kurtz et al., 2009), stretching the limits of performance of prosthetic devices, both in longevity and functionality, has become necessary. To this end, a great deal of research has placed special emphasis on developing and testing new wear-resistant materials and mechanical designs (Nägerl et al., 2008; Grupp et al., 2010; Grupp et al., 2013; Mantripragada et al., 2013). Numerical modeling has also played its part in guiding the direction of research and innovation (Haut Donahue et al., 2002; Halloran et al., 2005). However, to the best of the authors' knowledge, a detailed description of the behavior of the COF during all phases of a walking cycle is still missing, and required to further new developments in TKR design. For instance, through the behavior of the COF it is possible to infer the lubrication regimes under which the tribosystem operates; this information, in turn, may be used to improve upon the design of individual components of a TKR to reduce friction and wear.

The ISO 14243-3:2014 standard, to be referred to in the present work as the ISO standard, specifies the conditions for the wear testing of TKRs in wear-testing machines with displacement control (ISO 14243-3, 2014). Naturally, devices that actually comply with all the requirements of the ISO standard are quite complex, difficult to operate, and hinder the possibility of separately investigate tribological phenomena involved in the wear process, such as friction and lubrication.

Several apparatuses have been put forward to investigate tribological effects occurring in TKRs under *clinically relevant conditions*. Studies by Saikko et al. (2001), van Citters et al. (2004), and Patten et al. (2013), report on using simpler configurations to study wear in UHMWPE. For the study of lubrication, pin-on-disc (Heuberger et al., 2005) and ball-on-disc (Fan et al., 2011) configurations have been reported. With due care, these experimental setups have been proven to be suited for studying tribological effects occurring in more complex simulators. It is worth emphasizing that the use of simpler apparatuses has been performed, so far, without necessarily having in mind compliance with any ISO standard; rather, they have been applied around small regions of the COF-lubrication regime phase-space, in so called *clinically relevant conditions*, which are usually chosen as extremal conditions of prosthesis operation.

The primary objective of the present program is to establish an experimental method by means of which the operating conditions of loading and arthrokinematics prescribed by the ISO 14243-3:2014 standard for a TKR, are reproduced on a simplified geometry – an AISI 316L stainless steel ball on an ultra-high molecular weight polyethylene (UHMWPE) disc – to observe the behavior of the COF along an entire walking cycle.

2. Materials and methods

2.1. Experimental setup

The apparatus used in this investigation was an MTM2 ball-on-disc tribometer (PCS Instruments, London, UK). A schematic representation of the apparatus is shown in Fig. 1. The steel ball, loaded against the face of the UHMWPE disc, is driven independently from it, in direct or reverse motion, to create a mixed sliding/rolling condition determined by two parameters: the sliding-to-rolling ratio SRR and the entrainment speed $V_m = (V_1 + V_2)/2$, where V_1 and V_2 are the speed values of disc and ball at the contact point. The SRR is defined as the ratio $SRR = \left|V_r/V_m\right|$, where $V_r = V_1 - V_2$, is the relative velocity. The absolute value of SRR is obtained operationally by exchanging the speed values between disc and ball during measurement.

The frictional force between ball and disc is measured by a force transducer, while additional sensors measure applied load L and lubricant temperature. The tribopair consists of a 19.05 mm diameter AISI 316 L stainless steel ball, grade 100, with nominal roughness less than 0.012 μm, and a UHMWPE disc of 46 mm diameter and 6.00 ± 0.02 mm thickness.

2.2. Sample disc preparation

Slices of 6 mm thickness were cut from an as received 50.8 mm diameter UHMWPE white UVH bar, manufactured according to the ASTM-F648 standard. The thickness of the discs was rectified to 6.00 ± 0.02 mm and the diameter lathed down to 46 mm. The flat faces of the discs thus obtained were wet ground in running water with emery paper up to 1200 grit size. The average surface roughness R_a (0.025 ± 0.016 μm) was determined using an EasyScan2 atomic force microscope (Nanosurf, Liestal, Switzerland) operating in air, under ambient conditions.

2.3. Lubricant test fluid

Fetal bovine serum (FBS) S1650 from Biowest (Biowest SAS, Nuaillé, France) was used to prepare the testing lubricant fluid, following indications from the ISO standard. The testing lubricant solution was prepared by diluting the as received FBS in deionized, sterilized water until obtaining a final

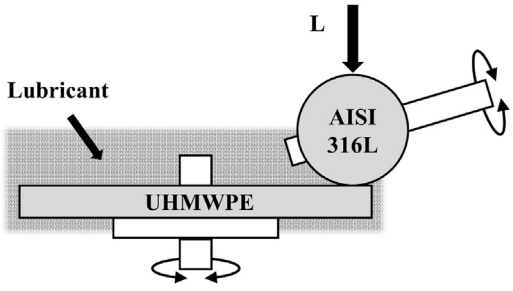

Fig. 1 – Schematic of the experimental setup indicating the load L applied during measurement. Both the UHMWPE disc and the AISI 316L ball rotate independently.

Table 1 – Protein concentration of the lubricants.

	Protein concentration (g/L)	Albumin (g/L)	α-Glob (g/L)	β-Glob (g/L)	γ-Glob (g/L)	Viscosity (mPa s)
As received	36	9.7	14.7	11.2	0.3	1.88
Diluted	20	5.37	8.14	6.21	0.17	1.54

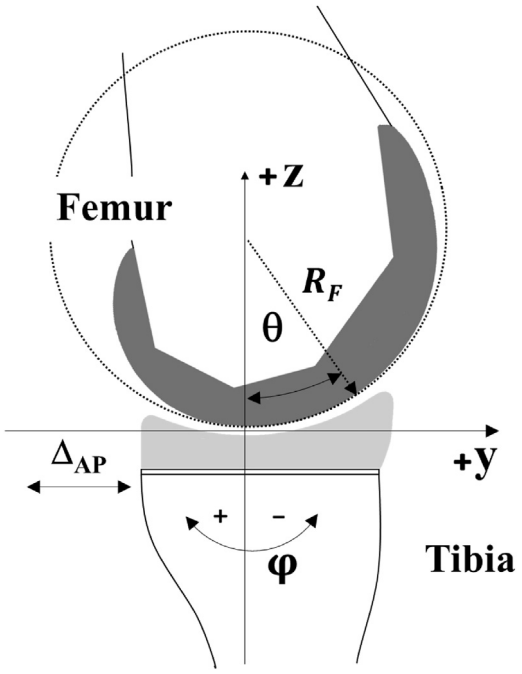

Fig. 2 – Arthrokinematics of a left TKR along a sagittal plane passing through the bottom of the tibial plateau of the medial tibial compartment, according to the ISO standard.

concentration of 20 g/L, as detailed in Table 1. No additional buffers or antimicrobial reagents were used. The test fluid's rheological behavior was characterized by means of a Physica MCR 101 rheometer (Anton Paar Gmbh, Graz, Austria), using the plate-on-plate configuration. Viscosity curves were acquired as a function of shear rate, between 10 and 1000 s^{-1}, using a 25 mm diameter plate and a 0.5 mm gap between plates, at 37 °C. For both fluids the viscosity shows a shear rate dependency; their values were almost constant from 800 s^{-1} onwards, being around 1.88 and 1.54 mPa·s for the as received FBS and the diluted solution, respectively.

2.4. *Adapting ISO standard requirements to the ball-on-disc experimental setup*

The arthrokinematics of a left TKR is schematically depicted in Fig. 2, along a sagittal plane passing through the bottom of the medial tibial plateau. The linear anterior–posterior displacement, the tibial rotation, and the flexion angle have been labeled as Δ_{AP}, φ, and θ, respectively. For a left TKR, according to the standard, θ is positive for flexion, φ is negative when rotating counter-clockwise and Δ_{AP} is positive when moving forward.

The location and direction of the axial force F_A and reaction forces F_L and F_M, acting on the lateral and medial

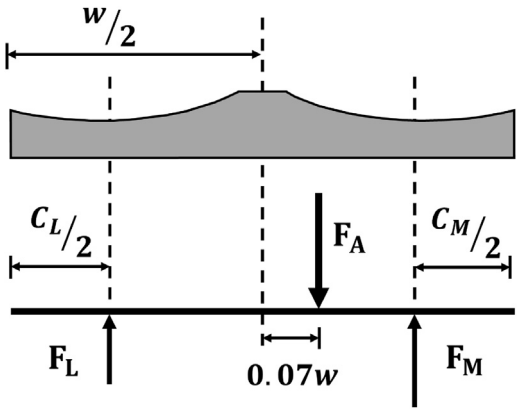

Fig. 3 – Free body diagram of axial (F_A) and reaction forces (F_L and F_M) acting on the tibial insert.

compartments of a tibial insert of a fixed-bearing knee-prosthesis, are schematically shown in Fig. 3. The distribution of the axial force between lateral and medial condyles keeps the proportion 39% to 61%. The reaction force F_M lies on the sagittal plane of Fig. 2, at a distance $C_M/2$ of the outer edge of the prosthesis of width w.

Reproducing the arthrokinematics and loading conditions indicated by the ISO standard on the ball-on-disc tribometer requires the geometric factors of the medial condyle for the specific TKR model used. To obtain them, a 3D model of the femoral and tibial components of a NexGen® CR-Flex Zimmer (Zimmer Inc., Warsaw, USA) fixed-bearing knee-prosthesis was obtained, using a Zscanner 800 3D scanner (Z Corporation, Rosemount, USA). Then, the required geometrical factors were obtained from the 3D models using commercially available CAD software.

2.4.1. *Loading conditions*

Due to the different values of curvature radii for femoral condyles and tibial compartments, the contact area at the tibiofemoral conformity area is elliptical, while it is circular for the ball-on-flat configuration. Therefore, the first step in adapting ISO standard conditions to the tribometer configuration was to establish equivalent conditions of contact pressure for both the TKR and the ball-on-flat setup. This was achieved by using Hertz's contact theory (van Beek, 2006) and appropriate values for the materials properties and geometric factors, indicated in Table 2.

The geometric factors were obtained from the 3D-scan models of the TKR. For the femoral component the curvature radius along the coronal plane was determined to be 38 mm, and along the sagittal plane, a value of 32.8 mm was assigned for the radius R_F of the *functional flexion–extension axis* (Asano et al., 2005), used later on to calculate the instantaneous

velocity V_F of the femoral component at the contact point. As for the concave medial compartment of the tibia, a value of –48.5 mm was determined for the radii of curvature along both the sagittal and coronal planes.

The mean contact pressure P_M for the prosthesis was obtained using the variation of F_M indicated by the standard, together with the calculated elliptical contact area at the tibial plateau obtained from the 3D model. The polycentric pathway followed by the radius of curvature of the femoral component during flexion–extension was taken into account (Gunston, 1971). The result is shown in Fig. 4 as a continuous line corresponds to the maximum contact pressure $P_{max}=1.5P_M$. The variations of the radius of curvature during the swing phase are reflected in the hump observed at the end of the prosthesis pressure curve.

Once the pressure P_M was obtained, the equivalent pressure P_L for the ball-on-disc configuration was calculated using the materials properties and geometric factors indicated in Table 2, correcting for the change in geometry of the contact area. Due to instrumental limitations, only integer values of load larger than 1 N were allowed. The load values L consistent with this restriction are shown as open squares in Fig. 4. In spite of the instrumental shortcoming, there is good agreement between the prosthesis pressure P_M, obtained from the ISO standard, and the working values for the tribometer pressure P_L, represented as black circles in Fig. 4, except at the end of the cycle, where the load L could not go any lower in the tribometer.

Table 2 – Materials properties and geometric factors of femoral and tibial components, and ball and disc tribopair.

	Medial condyle/Ball	Tibial insert/Disc
	Materials properties	
Roughness, R_a	0.012 μm	0.025±0.016 μm
Elasticity modulus, E	200 GPa	830 MPa
Poisson's ratio, ν	0.3	0.46
	Geometric factors	
Coronal radius (mm)	38/9.5	−48.5/∞
Sagittal radius (mm)	32.8/9.5	−48.5/∞

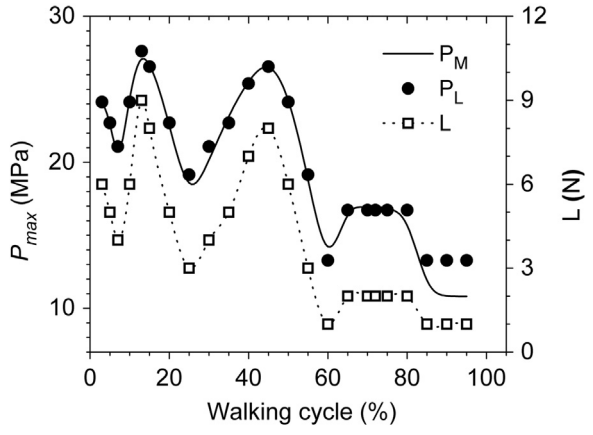

Fig. 4 – Contact pressure plots for both P_M and P_L on the prosthesis medial compartment and ball-on-disc tribometer, respectively. Also shown is the load L applied on the tribometer.

2.4.2. *Arthrokinematics of the TKR*

Using the arthrokinematics depicted schematically in Fig. 2 and the geometric factors in Table 2, the entrainment and relative speed between femur and tibia surfaces at the contact point $C_M/2$, in Fig. 3 were determined; these were labeled V_m and V_r, respectively. The instantaneous velocity V_F of the femoral component at the contact point was calculated for the entire walking cycle in time intervals of $\Delta t=0.01$ s, based on the ISO standard, using the radius of the functional flexion–extension axis $R_F = 32.8$ mm.

The velocity V_T of the tibial insert at the contact point has two components: one due to the AP-displacement Δ_{AP}, and the other one due to the internal–external rotation φR, where $R=22.1$ mm corresponds to the distance from the tibial axis to the bottom of the tibial plateau, as illustrated in Fig. 5 for a left TKR.

When divided by the time interval $\Delta t=0.01$ s, the velocity of the tibial plateau surface as a function of time $V_T(t)$ is given by:

$$V_T = \frac{\Delta_{AP} + \varphi R}{\Delta t}. \quad (1)$$

Once V_F and V_T are found, the relative and entrainment speeds are given, respectively, by:

$$V_r = V_F - V_T \quad (2)$$

and

$$V_m = \frac{V_F + V_T}{2}. \quad (3)$$

Finally, the sliding-to-rolling ratio SRR is:

$$SRR = \left| \frac{V_r}{V_m} \right| \quad (4)$$

In terms of SRR and V_m, the femoral and tibial speeds are given by: $V_{F,T} = V_m\,(1+SRR/2)$ and $V_{T,F} = V_m\,(1-SRR/2)$. The subindices emphasize the fact that, during the experiments, femoral and tibial speeds – executed by ball and disc, respectively – are exchanged.

2.4.3. *Kinematics for the ball-on-disc tribometer*

Using the geometric parameters in Table 2, the kinematics of the ball-on-disc configuration was determined, at 0.05 s

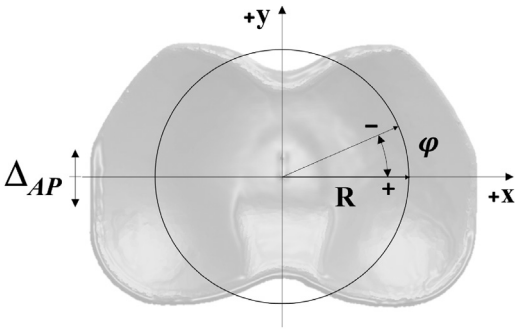

Fig. 5 – Arthrokinematics of the tibial insert of a left TKR according to the ISO standard, $R=22.1$ mm for the prosthesis model used in the present work.

intervals, from the arthrokinematics of femoral and tibial components in Fig. 6a, flexion points as well as local extrema of the curves were also included, tallying 24 experimental points from which V_r and V_m were obtained. Finally, SRR was calculated according to Eq. (4) using V_r and V_m in Fig. 6b. The SRR and V_m values fed to the ball-on-disc tribometer to measure the COF are shown in Fig. 7.

From Eqs. (2), (3) and (4), it is possible to obtain the conditions for which either sliding or rolling motions dominate: for SRR ≥ 2, both surfaces move in opposite directions. In this case, sliding is the predominant mode of motion, being SRR=2 the onset for it. On the other hand, for SRR<2 both surfaces move in the same direction. In this case, the motion is dominated by rolling. The condition for which SRR=0, corresponds to pure rolling.

3. Results

3.1. *Friction coefficient in the walking cycle*

Following the prescribed method, the COF was measured for the as received FBS and the diluted solution of Table 1. Every (L, V_m, SRR) triad of values was set in the tribometer, centering the desired value of entrainment speed within the interval $V_m \pm 5$ mm/s to obtain the COF under steady conditions. The variation of the COF over an entire walking cycle is shown in Fig. 8; the bars in this figure represent the standard error of the means.

Two friction regimes are distinguished: low-friction for the stance phase and high-friction for the swing phase, the transition from one to the other takes place from the pre-swing to the initial swing phases of the cycle. Similar behavior was observed for both the as-received and diluted test fluids. Slightly higher values of COF along the entire cycle were measured for the as received FBS.

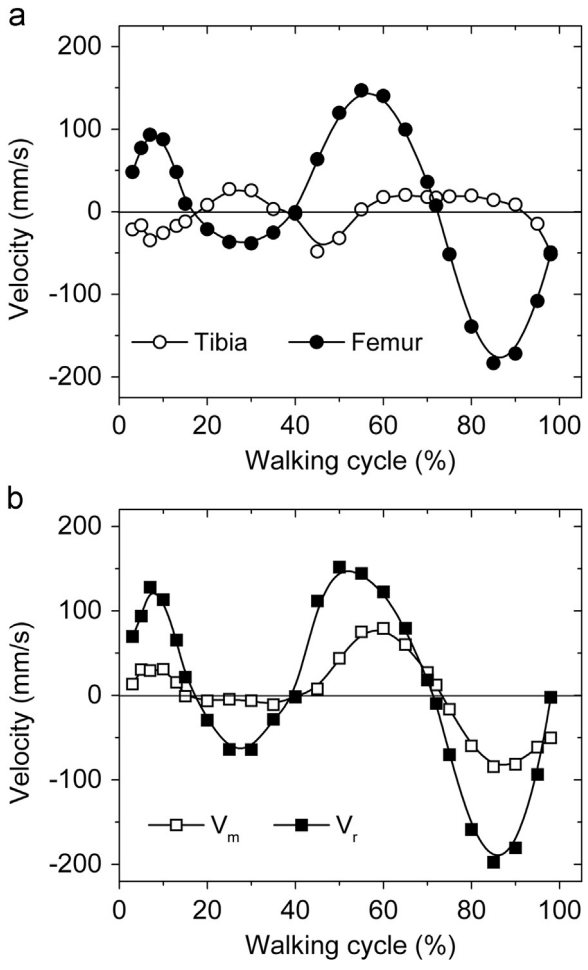

Fig. 6 – (a) Velocities of femur and tibia surfaces, and (b) entrainment and relative velocities for a walking cycle, based on the ISO standard, using the geometric factors of the TKR 3D-model.

4. Discussion

As observed in Fig. 8, the COF is lower for the diluted lubricating fluid along the whole walking cycle. This result furthers the idea that a protein mediated lubricating mechanism is at work in the tribosystem and will be used to explain some of the general features observed.

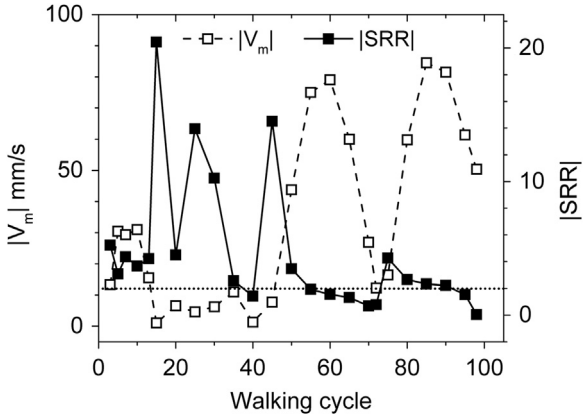

Fig. 7 – Sliding-to-rolling ratio values obtained from Fig. 6b, and corresponding |Vm| for the entire walking cycle.

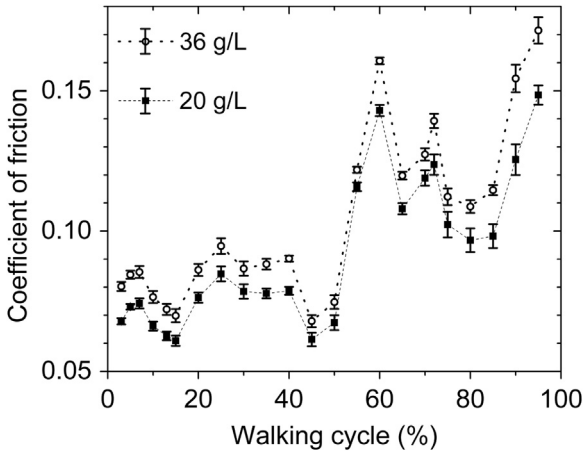

Fig. 8 – Behavior of the COF for the lubricant fluids at two concentrations: 36 g/L (undiluted) and 20 g/L (diluted), for the entire walking cycle.

Table 3 – Coefficients and powers of the regression model for both lubricants.

	$COF = b_0 P^{b_1} \lvert SRR \rvert^{b_2}$			
	b_0	b_1	b_2	R^2
COF (@ 20 g/l)	1.319	-0.873	-0.090	0.89
COF (@ 36 g/l)	1.575	-0.893	-0.084	0.92

During the stance phase, the COF is lower than during the swing phase, even though the average load is higher in the former, an effect contrary to EHL lubrication theory. Furthermore, this transition starts at the pre-swing phase and coincides with two events: a drop in F_M (Fig. 4), and a decrease in SRR below 2 (Fig. 7).

Since the COF values reported in the literature correspond to narrow regions of parameters *clinically relevant*, no data are available to compare with the results obtained in the present work, for the entire walking cycle. Nonetheless, the dependence of the COF on the experimental parameters: V_m, SRR, and P, was investigated statistically, via standard regression analysis, adopting a significance level $\alpha = 0.05$ to decide on whether or not the variables had a significant effect on the COF.

Some of the analyzed linear models required up to five adjusting parameters to provide determination coefficients R^2 of about 0.90. Nonetheless, a power model of the type

$$COF = b_0 P^{b_1} \lvert SRR \rvert^{b_2} \lvert V_m \rvert^{b_3} \quad (5)$$

also produced determination coefficients close to 0.90, and the corresponding ANOVA showed that $|V_m|$ had no significant effect on the COF for either of the testing fluids. A summary of the statistical results is shown in Table 3.

The exponent of P is an order of magnitude larger than the exponent of |SRR|, which means that the COF changes much faster with P than with |SRR|. The merit of this model is that it explains 90% of the variability of the COF with a reduced number of parameters, as shown in Fig. 9.

The model fits quite well for both protein concentrations, especially during the stance phase when P and |SRR| reach their highest values. Well within the swing phase, between 60% and 80% of the walking cycle, there is good agreement between the two plots. Towards mid-swing, however, the discrepancy between model and experimental COF is accentuated. Still, the value of this result is that it provides a useful model for numerical simulations of friction and wear of UHMWPE lubricated with FBS.

A mathematical model of wear in a TKR could use Eq. (5) to completely define the stress state of UHMWPE at the contact point. The von Mises yield parameter maximum, on the surface and the subsurface, increases as the COF reaches higher values; furthermore, the maximum yield parameter below the surface moves towards the surface as COF increases, which makes the material more prone to fail (Hamilton, 1983).

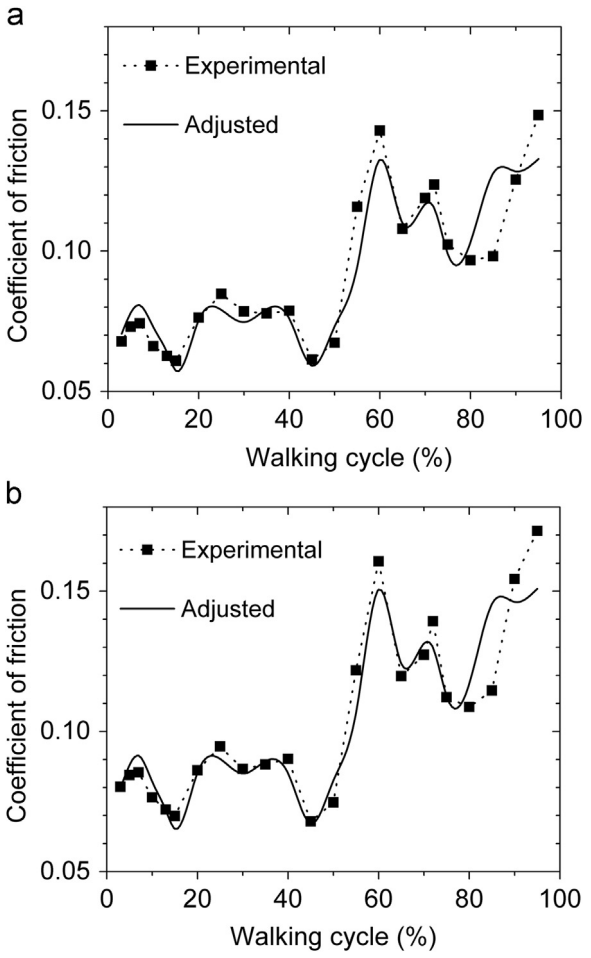

Fig. 9 – Power model of the COF for concentrations of (a) 20 g/L, and (b) 36 g/L.

5. Conclusions

By successfully translating ISO 14243:2014 arthrokinematics into a ball-on-disc configuration, it was possible to measure the COF throughout an entire walking cycle.

In contrast to most methods described in the reviewed literature, the one prescribed in the present work permits the systematic exploration of the effect of geometric and dimensional changes in the individual components of the tribosystem, over a wider range of the tribological parameters than the ones limited to *clinically relevant* conditions.

Acknowledgments

The authors gratefully acknowledge the support from the Instituto Politécnico Nacional, through grants SIP20131650 and SIP20151552, and the National Council for Science and Technology (CONACYT) through grants 106284 and 248639. M. Alvarez-Vera and L.A. Montoya-Santiyanes also acknowledge economic support from the same source to carry on post-doctoral and graduate studies, respectively.

REFERENCES

Asano, T., Akano, M., Nakamura, T., 2005. The functional flexion-extension axis of the knee corresponds to the surgical epicondylar axis: in vivo analysis using a biplanar image-matching technique. J. Arthroplast. 20 (8), 1060–1067, http://dx.doi.org/10.1016/j.arth.2004.08.005.

Fan, J., Myant, C.W., Underwood, R., Cann, P.M., Hart, A., 2011. Inlet protein aggregation: a new mechanism for lubricating film formation with model synovial fluids. Proc. IMech E 225 H: J. Eng. Med. pp. 696–709.

Grupp, T.M., Utzschneider, S., Schröder, C., Schwiesau, J., Fritz, B., Maas, A., Blömer, W., Jansson, V., 2010. Biotribology of alternative bearing materials for unicompartmental knee arthroplasty. Acta Biomater. 6, 3601–3610, http://dx.doi.org/10.1016/j.actbio.2010.04.003.

Grupp, T.M., Giurea, A., Miehlke, R.K., Hintner, M., Gaisser, M., Schilling, C., Schwiesau, J., Kaddick, C., 2013. Biotribology of a new bearing material combination in a rotating hinge knee articulation. Acta Biomater. 9, 7054–7063, http://dx.doi.org/10.1016/j.actbio.2013.02.030.

Gunston, F.H., 1971. Polycentric knee arthroplasty Prosthetic simulation of normal knee movement. J. Bone Jt. Surg. 53B (2), 272–277.

Halloran, J.P., Petrellab, A.J., Rullkoettera, P.J., 2005. Explicit finite element modeling of total knee replacement mechanics. J. Biomech. 38, 323–331, http://dx.doi.org/10.1016/j.jbiomech.2004.02.046.

Hamilton, G.M., 1983. Explicit equations for the stresses beneath a sliding spherical contact. Proc. Inst. Mech. Eng. 197C, 53–59.

Haut Donahue, T.L., Hull, M.L., Rashid, M.M., Jacobs, C.R., 2002. A finite element model of the human knee joint for the study of tibio-femoral contact. J. Biomech. Eng. 124, 273–280, http://dx.doi.org/10.1115/1.1470171.

Heuberger, M.P., Widmer, M.R., Zobeley, E., Glockshuber, R., Spencer, N.D., 2005. Protein-mediated boundary lubrication in arthroplasty. Biomaterials 26, 1165–1173, http://dx.doi.org/10.1016/j.biomaterials.2004.05.020.

ISO 14243-3, 2014. Implants for surgery - Wear of total knee-joint prostheses - Part 3: Loading and displacement parameters for wear-testing machines with displacement control and corresponding environmental conditions for test, second edition International Organization for Standardization, Geneva, Switzerland.

Kurtz, S.M., Lau, E., Ong, K., Zhao, K., Kelly, M., Bozic, K.J., 2009. Future young patient demand for primary and revision joint replacement: national projections from 2010 to 2030. Clin. Orthop. Relat. Res. 467, 2606–2612, http://dx.doi.org/10.1007/s11999-009-0834-6.

Kurtz, S.M., 2009. The clinical performance of UHMWPE in knee replacements. In: Kurtz, S.M. (Ed.), UHMWPE Biomaterials Handbook 2nd edition Elsevier, China, pp. 97–115.

Mantripragada, V.P., Lecka-Czernik, B., Ebraheim, N.A., Jayasuriya, A.C., 2013. An overview of recent advances in designing orthopedic and craniofacial implants. J. Biomed. Mater. Res. Part A 101A, 3349–3364, http://dx.doi.org/10.1002/jbm.a.34605.

Nägerl, H., Frosch, K.H., Wachowski, M.M., Dumont, C., Abicht, Ch, Adam, P., Kubein-Meesenburg, D., 2008. A novel total knee replacement by rolling articulating surfaces. In vivo functional measurements and tests. Acta Bioeng. Biomech. 10 (1), 55–60.

Patten, E.W., van Citters, D., Ries, M.D., Pruitt, L.A., 2013. Wear of UHMWPE from sliding, rolling, and rotation in a multidirectional tribosystem. Wear 304, 60–66, http://dx.doi.org/10.1016/j.wear.2013.04.017.

Saikko, V., Ahlroos, T., Calonius, O., 2001. A three-axis knee wear simulator with ball-on-flat contact. Wear 249, 310–315, http://dx.doi.org/10.1016/S0043-1648(01)00567-1.

van Beek, Anton, 2006. Advanced Engineering Design. Delft University of Technology, The Netherlands.

van Citters, D.W., Kennedy, F.E., Currier, J.H., Collier, J.P., Nichols, T.D., 2004. A Multi-station rolling/sliding tribotester for knee bearing materials. Trans. ASME 126, 380–385, http://dx.doi.org/10.1115/1.1645536.